Tensorial Electrokinetics in Articular Cartilage

Boris Reynaud and Thomas M. Quinn
Cartilage Biomechanics Group, Ecole Polytechnique Fédérale de Lausanne, Lausanne, Switzerland

ABSTRACT Electrokinetic phenomena contribute to biomechanical functions of articular cartilage and underlie promising methods for early detection of osteoarthritic lesions. Although some transport properties, such as hydraulic permeability, are known to become anisotropic with compression, the direction-dependence of cartilage electrokinetic properties remains unknown. Electroosmosis experiments were therefore performed on adult bovine articular cartilage samples, whereby fluid flows were driven by electric currents in directions parallel and perpendicular to the articular surface of statically compressed explants. Magnitudes of electrokinetic coefficients decreased slightly with compression (from ~ -7.5 μL/As in the range of 0–20% compression to -6.0 μL/As in the 35–50% range) consistent with predictions of microstructure-based models of cartilage material properties. However, no significant dependence on direction of the electrokinetic coupling coefficient was detected, even for conditions where the hydraulic permeability tensor is known to be anisotropic. This contrast may also be interpreted using microstructure-based models, and provides insights into structure-function relationships in cartilage extracellular matrix and physical mediators of cell responses to tissue compression. Findings support the use of relatively simple isotropic modeling approaches for electrokinetic phenomena in cartilage and related materials, and indicate that measurement of electrokinetic properties may provide particularly robust means for clinical evaluation of cartilage matrix integrity.

INTRODUCTION

The biomechanically functional extracellular matrix of articular cartilage is a hydrated polyelectrolyte gel containing fixed negative charges on proteoglycans enmeshed within a collagen network, with corresponding positive charges in the matrix fluid (1,2). Tissue deformations induce relative motion between matrix fluid and solid, giving rise to electrokinetic phenomena including electric streaming potentials that accompany pressure-driven fluid flows (3,4), and electroosmotic fluid flows driven by electric current (5). These phenomena reflect coupling between fluid-solid relative motion and electric charge transport, which occurs in many contexts (6,7). Electrokinetic phenomena contribute to functions of many biological tissues (2) and have practical applications including microfluidics (8) and control of molecular filtration (9–11).

In cartilage, electrokinetic phenomena depend upon the concentration of glycosaminoglycans immobilized in the matrix (12,13). Changes in this matrix component are among the earliest events in osteoarthritic cartilage degradation (14). In situ measurements of electromechanical coupling (15–17) and electric conductivity (18,19) therefore carry promise for early detection of focal cartilage lesions. Accurate theoretical modeling of cartilage electromechanics (20–22) can be important for interpretation of such measurements. Characterization of electrokinetic properties of compressed cartilage therefore supports accurate application of electrically based measurements of cartilage integrity.

Electrokinetic transport phenomena may also mediate cell biological responses to tissue compression (23). The extracellular matrix of adult articular cartilage is avascular, and chondrocytes rely upon interstitial solute transport for acquisition of nutrients, rejection of wastes, intercellular signaling, and matrix remodeling (1). Solute transport is influenced by changes in matrix composition (24) and structure (25,26), fluid flows (27), and associated electrokinetic phenomena (5). Fields, forces, and flows around individual chondrocytes may therefore influence their responses to cartilage compression (23,28) by modulation of solute transport. Elucidation of relationships between cartilage matrix deformations and electrokinetic phenomena therefore improves understanding of cartilage physiology and may lead to improved tissue repair methods.

During compression, cartilage glycosaminoglycans are thought to change their orientations and relative positions such that matrix molecular architecture can acquire direction-dependent features though none exist in unloaded tissue (29). Such changes appear to underlie the emergence of anisotropy (direction-dependence) in the hydraulic permeability tensor of cartilage with increasing compression (30). Because electrokinetic transport phenomena are also governed by matrix glycosaminoglycans (2,31), it is reasonable to hypothesize that these properties may also become anisotropic with cartilage compression. Such changes could mediate cell responses to cartilage compression, including direction-dependent pericellular matrix deposition (28). Furthermore, though the inhomogeneities of cartilage electrokinetic properties have been explored somewhat (4), relatively little is known regarding their anisotropies (32).

The direction-dependent tensorial character of cartilage electrokinetic transport properties is therefore important to

Submitted January 30, 2006, and accepted for publication June 12, 2006.

Address reprint requests to Thomas M. Quinn, PhD, Cartilage Biomechanics Group, AI 1234 EPFL Station 15, CH-1015 Lausanne, Switzerland. Tel.: 41-21-693-83-50; Fax: 41-21-693-86-60; E-mail: thomas.quinn@epfl.ch.

0006-3495/06/09/2349/07 $2.00

doi: 10.1529/biophysj.106.082263

understanding tissue physiology and for clinical evaluation of matrix integrity. Our goals were to examine this direction-dependence by performing electroosmosis experiments on compressed cartilage explant disks. Experiments were designed such that electrokinetic properties could be measured in multiple directions within individual statically compressed explants, to highlight compression-dependent, anisotropic behavior despite variations in composition and structure.

METHODS

Experimental methods

Refrigerated humeri of 18-month-old cows were obtained within 24 h of slaughter. Osteochondral cores of 4 mm diameter were taken from the proximal articular surface using a biopsy drill and bone saw (Stratec, Oberdorf, Switzerland) under irrigation with phosphate buffered saline ((PBS); without Ca^{2+} or Mg^{2+}). Using a microtome (Leica RM 2135, Wetzlar, Germany), a superficial layer ~100-μm thick was removed then a disk ~1000-μm thick was cut consisting primarily of intermediate zone cartilage. The disk axial direction corresponded to that perpendicular to the articular surface, whereas the radial direction corresponded to the parallel direction. Explants were stored at −20°C in PBS containing protease inhibitors (complete tablets, Boehringer Mannheim, Basel, Switzerland) and 0.1 mg/ml sodium azide (Sigma, St. Louis, MO), then defrosted for 2 h in PBS before experiments. Free-swelling explant thicknesses were measured under a dissection microscope and used as references for compressive strain.

Explant disks were sandwiched between two precision-machined plexiglass blocks. Along the explant axis, 2.35 mm diameter × 2 mm thick rigid porous cylinders (laser machined from Al_2O_3 0.5-μm pore size cut-off filters; Kerafol GmbH, Eschenbach, Germany) were mounted flush inside the plexiglass blocks, providing conduits to PBS reservoirs (Fig. 1). Both plexiglass blocks also contained 4 mm diameter × 100 μm deep recesses to keep explants centered during mounting and compression. An O-ring around explants functioned as a gasket. Between the explant radial boundary and O-ring, another porous ceramic cylinder was mounted in the lower plexiglass block, leading to another PBS reservoir. Care was taken during assembly to avoid air bubbles inside the apparatus. The explant represented the only source for electroosmotic fluid flow. Each of the three PBS reservoirs branched into paths for electric current and fluid flow (Fig. 2). Electric current paths consisted of a 10% polymethacrylate (PMA) gel cast within a silicone rubber tube of length 10 cm and inner diameter 3.2 mm (MasterFlex, Cole-Parmer Instrument, Vernon Hills, IL) leading to a 50-μm × 5 mm × 20 mm platinum sheet electrode (Johnson-Matthey, London, UK) partially immersed in a 200-mL PBS bath. PMA gels served as salt bridges to inhibit transport of electrode reaction products to the cartilage disk, and as high flow-resistance elements to force fluid flows into separate paths. Above the cartilage explant, the fluid flow path consisted of a silicone rubber tube leading to a fourth 200 mL PBS bath. Fluid flow through the explant lower axial surface (axial outflow) and through the explant radial edge (radial outflow) were directed into glass capillaries (Figs. 1 and 2) of 340-μm inner diameter (Drummond Scientific, Broomall, PA) leading to atmospheric conditions.

The plexiglass blocks were held together by aluminum plates with central openings allowing observation of cartilage explants. Screws between the plates were tightened uniformly to statically compress explants. After mounting in the apparatus under a relatively small compression (≤25%), explant geometry was measured using a microscope (Zeiss LSM 410, Jena, Germany) with 20× objective and motorized stage. Disk diameter was quantified by stage displacements whereas thickness was determined by changes in focal depth between plexiglass surfaces bounding the explant (accounting for the indices of refraction of air and PBS). The apparatus was then placed on the motorized stage (Scan IM 100 × 100 and MultiControl 2000, ITK Kassen GmbH, Lahnau, Germany; interfaced with LabVIEW, National Instruments) of another microscope (Zeiss Axiovert 100) and left for 4–12 h without applied electric currents. To minimize temperature fluctuations the apparatus was surrounded by a styrofoam freezer box lined with plastic tubing through which water at 18.5°C flowed in series with a fixed-temperature recirculator (model 18205, Fischer Bioblock Scientific, Illkirch, France).

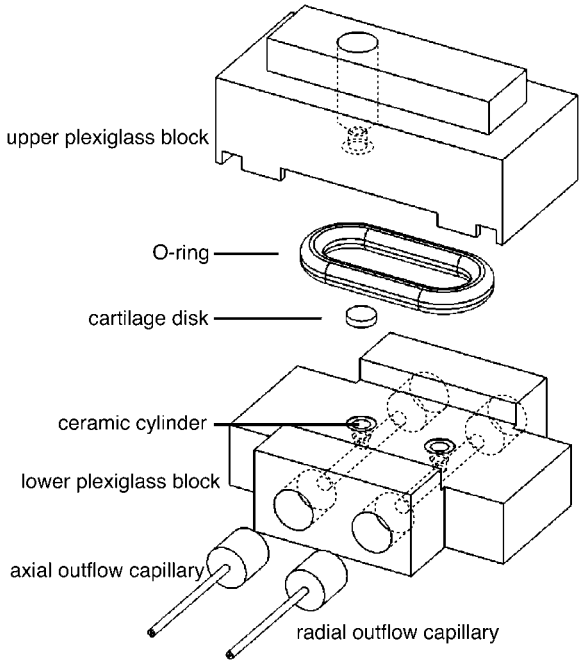

FIGURE 1 Exploded view of apparatus used to measure electrokinetic fluid transport in statically compressed cartilage explants. Cylindrical explant disks were sandwiched between precision-machined plexiglass blocks. Dotted lines indicate conduits for currents and fluid flows through the apparatus. Above and below explants, 2.35-mm diameter porous ceramic disks were centered on the explant axis.

When PBS-air menisci in axial and radial outflow capillaries were stable for a few hours, an electric current (I) in the range $-150\ \mu A < I < 150\ \mu A$ was passed through the explant disk in either the axial or radial outflow direction (Fig. 2); current densities were similar to previous studies (5). Steady current (±0.1 μA) was delivered by a high-voltage supply (Keithley model 248, Keithley Instruments, Cleveland, OH) in series with a 10-MΩ resistance. Positive currents induced positive fluid outflows (Fig. 2). Each time changed, current was held constant for 15 min or more while outflows were monitored using a charge-coupled device camera (Sony XC-75CE, Tokyo, Japan) and 10× objective. Menisci velocities and capillary cross-sectional areas provided volumetric outflow rates (Q). This procedure was

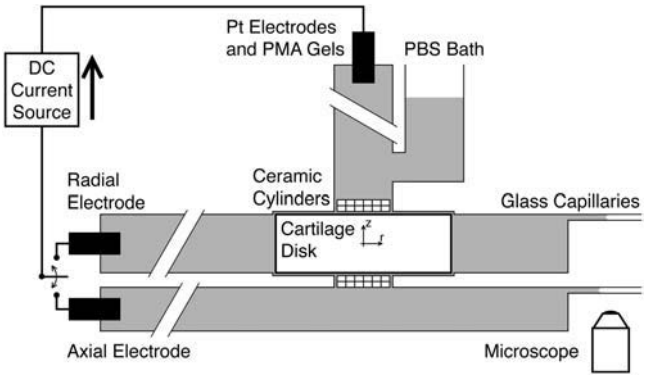

FIGURE 2 Schematic sketch of experimental apparatus.

repeated for four to six different applied currents (including zero; Fig. 3 *a*) providing axial and radial outflows versus applied current within individual compressed cartilage disks (Fig. 3 *b*). Static compression was then increased (to ~25–50%) and measurements repeated. Explants were used for at most 2 days.

A total of 11 explants were used from three different dissections. All explants contributed data at two static compression levels. Differences between electrokinetic coupling coefficients (defined below) in radial and axial directions were examined using *t*-tests for paired samples. Linear correlation analysis (Pearson's *r*) was used to quantify significance of trends versus static compression (33). Findings were considered significant for $p < 0.05$. Data are reported as mean ± SE (*n*).

Theoretical methods

Extending previous work (20,34,35), a tensorial description of electrokinetic phenomena in homogeneous porous materials may be summarized by a matrix relating area-averaged fluid velocity (**U**) and electric current density (**J**) vectors to gradients of fluid hydrostatic pressure (p) and electric potential (ϕ):

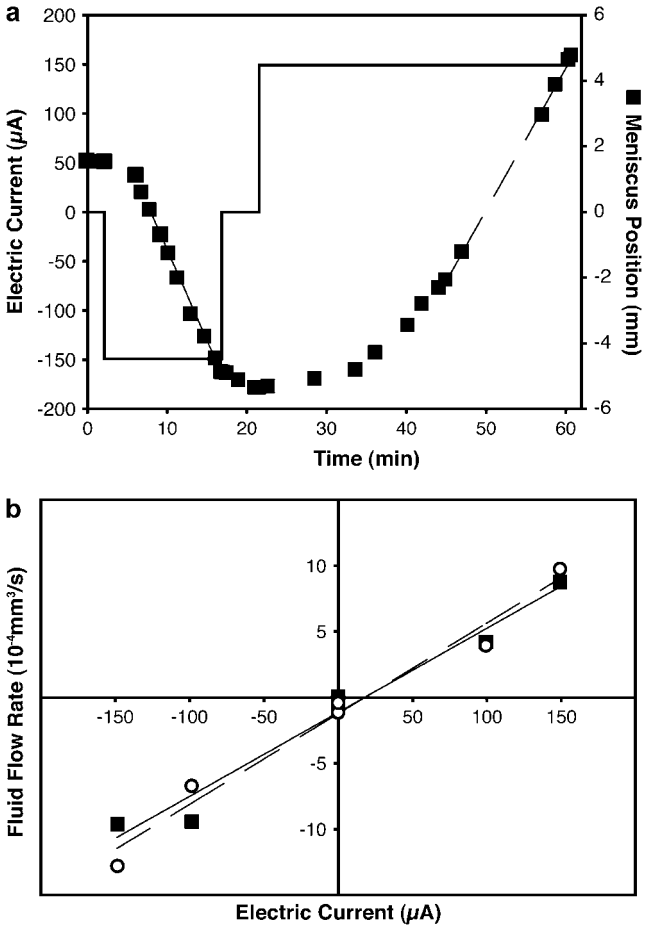

FIGURE 3 (*a*) Applied electric current and radial flow meniscus position versus time for a cartilage disk under 29% static compression. Dotted lines indicate regimes with constant currents and fluid flow rates. (*b*) Axial (○) and radial (■) fluid flow rates versus electric current for the same explant. Linearity of electrokinetic coupling is indicated by the solid line (linear fit) for radial flow and the dotted line for axial flow.

$$\begin{bmatrix} \mathbf{U} \\ \mathbf{J} \end{bmatrix} = \begin{bmatrix} -\mathbf{K}_{11} & \mathbf{K}_{12} \\ \mathbf{K}_{21} & -\mathbf{K}_{22} \end{bmatrix} \cdot \begin{bmatrix} \nabla p \\ \nabla \phi \end{bmatrix}. \quad (1)$$

Tensor components of this matrix include the ''short-circuit'' hydraulic permeability ($\mathbf{K}_{11}$), electric conductivity ($\mathbf{K}_{22}$), and the electromechanical coupling tensors ($\mathbf{K}_{12}$ and $\mathbf{K}_{21}$). The ''open circuit'' (Darcy) hydraulic permeability, relating **U** to ∇p in the common case where $\mathbf{J} = \mathbf{0}$, can be direction-dependent in compressed cartilage, with up to 10-fold greater permeability in the direction of compression (perpendicular to the articular surface) (30). Consistent with microstructure-based models of cartilage anisotropic material properties (29), principal axes of the ''open circuit'' hydraulic permeability appear to correspond to dominant directions defining tissue structure and function. Because all phenomenological tensor components arise from the same microstructure, we assume that all $\mathbf{K}_{ij}$ may be written

$$\mathbf{K}_{ij} = \mathbf{i}_r \mathbf{i}_r K_{ij}^r + \mathbf{i}_z \mathbf{i}_z K_{ij}^z, \quad (2)$$

where r and z denote directions parallel and perpendicular to the articular surface, $\mathbf{i}$ represents a unit vector, and the K_{ij}^x values are constant scalars (i, j, and x being dummy variables).

For one-dimensional (1-D) electroosmosis along a principal axis (denoted by x), fluid flows may be driven solely by electric potential gradients ($\nabla p = \mathbf{0}$) and the ratio between **U** and **J** defines the electrokinetic coupling coefficient (20) of magnitude

$$k_e^x = \frac{K_{12}^x}{K_{22}^x}. \quad (3)$$

The vector components of **U** and **J** are then simply related by

$$U_x = -k_e^x J_x. \quad (4)$$

Integrating both sides of Eq. 4 over a surface through which current and fluid pass perpendicularly during 1-D electroosmosis provides

$$Q_x = -k_e^x I_x, \quad (5)$$

where Q_x and I_x represent volumetric fluid flow rate and electric current across this surface. The electrokinetic coupling coefficient k_e^x may therefore be determined from macroscale measurements of Q_x and I_x, for a purely 1-D experiment.

For two-dimensional (2-D) electric currents and fluid flows as in this study, conservation of fluid volume and electric charge at steady-state imply

$$\nabla \cdot \mathbf{U} = \nabla \cdot \mathbf{J} = 0. \quad (6)$$

For the case of radial outflow (Fig. 2), current and volumetric fluid flow entering the explant through its upper axial surface must therefore equal those leaving through the radial surface. If $\mathbf{k}_e$ (a tensor with form as in Eq. 2 and components k_e^r and k_e^z) is isotropic, then pure electroosmotic flows ($\nabla p = \mathbf{0}$ everywhere) can be maintained because Eq. 5 may be consistently applied at both the inflow and the outflow surfaces. (The imposed current induces the same volumetric fluid flow into and out of the explant.) In contrast, if $\mathbf{k}_e$ is anisotropic similarly to the ''open circuit'' hydraulic permeability such that $k_e^z > k_e^r$ (for example), then constant electric current that changes from the axial to the radial direction will induce greater electroosmotic fluid flows in the axial versus the radial direction. To satisfy Eq. 6, pressure gradients would then arise to diminish axial fluid inflow and augment radial outflow, for this hypothetical case. Direction-dependence of $\mathbf{k}_e$ is therefore expected to manifest itself by differences in fluid outflow when constant electric current is switched between axial and radial cases (Fig. 2). If constant electric current is switched and fluid outflow remains unchanged, this indicates $k_e^z = k_e^r$.

These intuitive arguments may be formalized somewhat by using Eqs. 1–3 to write, as in previous work (20),

$$\mathbf{U} = -\mathbf{k}_e \cdot \mathbf{J} - \mathbf{K} \cdot \nabla p, \quad (7)$$

where **K** is the "open-circuit" hydraulic permeability tensor, with form as in Eq. 2 and components

$$K^{x} = K^{x}_{11} - \frac{K^{x}_{12}K^{x}_{21}}{K^{x}_{22}}. \quad (8)$$

Taking the divergence of both sides of Eq. 7, integrating the result over the explant volume for a radial outflow experiment, and applying Gauss' divergence theorem together with Eq. 6 then provides

$$(k^{z}_{e} - k^{r}_{e})I = [S_z K^{z}(\overline{\mathbf{i}_z \cdot \nabla p}) + S_r K^{r}(\overline{\mathbf{i}_r \cdot \nabla p})], \quad (9)$$

where I is the imposed current and $\overline{\mathbf{i}_x \cdot \nabla p}$ represents the mean value of the outward-directed component of ∇p over the inflow or outflow surface S_x. Equation 9 therefore illustrates that pressure gradients will arise if $k^{z}_{e} \neq k^{r}_{e}$, driving fluid flows that compensate for the difference between electro-osmotically driven flows into and out of the explant. In contrast, an axial outflow experiment is expected to be nearly 1-D in nature, with identical electrokinetic coupling coefficients at the inflow and outflow surfaces; therefore fluid flows in that case are nearly purely electroosmotic, and expected to differ from those of the radial flow case if $k^{z}_{e} \neq k^{r}_{e}$.

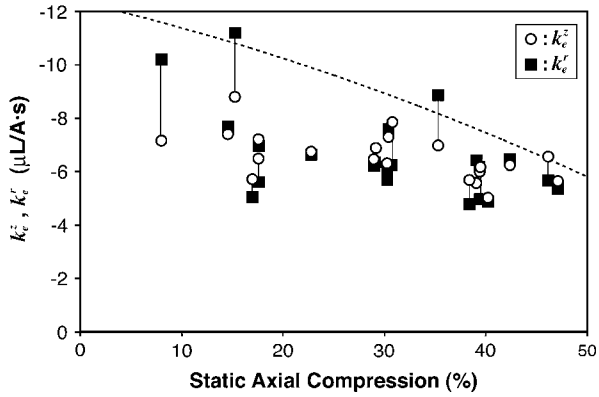

FIGURE 4 Electrokinetic coupling coefficients in the axial (k^{z}_{e}, ○) and radial (k^{r}_{e}, ■) directions of cartilage disks under varying levels of radially unconfined static axial compression. Lines connect data acquired from a single explant disk at one compression level. Dotted line indicates predicted k^{x}_{e} derived from results of an isotropic model of cartilage matrix electrokinetics (38).

RESULTS

When electric current was changed from 0 to 150 μA to the radial electrode (Fig. 2), radial fluid outflow reached a steady value after several minutes (Fig. 3 *a*). This transitional period was consistently shorter for negative than positive currents, and appeared to be the time required to attain adequate pressures to drive fluid flow through the capillary, where the asymmetric delay reflected nonlinear (tension versus compression) deformations in the PMA gel salt bridges. As previously described (20), unlike pressure-induced fluid flow, pure electroosmotic fluid flow does not intrinsically involve cartilage matrix deformations. Therefore, the observed delay (Fig. 3 *a*) was not necessarily related to mechanical relaxation within the cartilage explant itself. Furthermore, direct observation of explants during this transitional period did not reveal noticeable deformations.

Steady-state radial outflows attained (Fig. 3 *a*) after ~20 min could be maintained for several hours. Concomitantly, fluid flow through the axial outflow capillary was negligible while no current flowed to that electrode. When electric current was switched to the axial electrode (Fig. 2), axial outflow became nonzero whereas radial outflow was negligible. Steady-state flow regimes provided electroosmotic flow rates versus applied current (Fig. 3 *b*). For both axial and radial outflows, the relationship between Q and I appeared to be linear with similar slopes in the range $-150\ \mu A < I < 150\ \mu A$. Slight departures from zero flow rate at zero current (Fig. 3 *b*) reflected background noise, likely due to thermal effects. Control studies using 10% PMA gel in place of cartilage disks resulted in negligible fluid flow regardless of applied current, confirming that cartilage was the sole source for electroosmotic flow.

The slopes of Q versus I plots (Fig. 3 *b*) provided k^{r}_{e} and k^{z}_{e} (Eq. 5). The range of values (from -4.8 to -11.2 μL/As; Fig. 4) was consistent with previous 1-D measurements in uncompressed calf cartilage (5). Paired sample analysis detected no significant differences ($p > 0.05$) between k^{r}_{e} and k^{z}_{e} over the full range of data (Fig. 4), nor within the compression ranges 0–20%, 20–35%, and 35–50%. Both k^{r}_{e} and k^{z}_{e} exhibited significant linear correlations as decreasing functions of compression ($p \leq 0.01$). However, these decreases were not very dramatic over the range of compression applied (Fig. 4). Mean values of k_e (with k^{r}_{e} and k^{z}_{e} pooled together) measured within the compression ranges 0–20%, 20–35%, and 35–50% were -7.5 ± 0.5 ($n = 12$), -6.6 ± 0.2 ($n = 14$), and -6.0 ± 0.2 ($n = 18$) μL/As, respectively.

Anisotropy of k_e was also examined via the normalization k^{z}_{e}/k^{r}_{e} versus compression (Fig. 5). No significant differences between this quantity and 1 were evident for the full range of data nor within the compression ranges 0–20%, 20–35%,

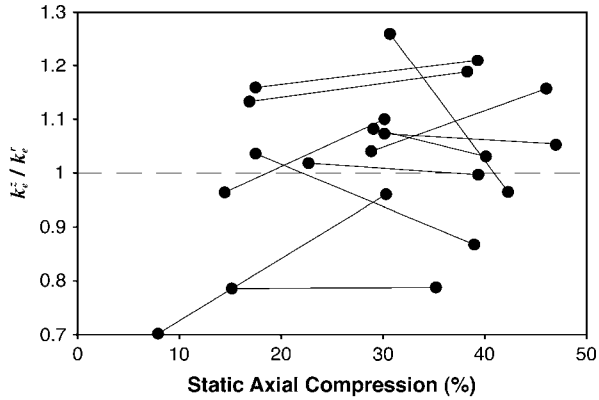

FIGURE 5 The ratio between axial and radial electrokinetic coupling coefficients (k^{z}_{e}/k^{r}_{e}) of cartilage disks under varying levels of radially unconfined static axial compression. Lines connect data acquired from a single explant disk.

and 35–50%. Furthermore, no significant linear correlation was detected between k_e^z/k_e^r and compression (Fig. 5).

DISCUSSION

Cartilage explant disks compressed axially up to 50% exhibited $\mathbf{k}_e$ with a weak dependence upon compression, but no detectable direction dependence ($k_e^z/k_e^r \approx 1$). The material properties governing electroosmotic flows therefore appear to be isotropic even when cartilage is highly compressed and other transport properties such as hydraulic permeability are markedly anisotropic (30). Measurements did not include superficial zone cartilage that bears a relatively high concentration of preferentially oriented collagen fibrils and therefore may exhibit more anisotropic properties. However, electrokinetic phenomena arise primarily within the proteoglycan gel, and it remains unclear to what extent collagen fibrils affect the anisotropies of the matrix electromechanical coupling tensor $\mathbf{K}_{12}$ and conductivity $\mathbf{K}_{22}$ differentially, such that $\mathbf{k}_e$ becomes significantly anisotropic. Therefore, these findings support relatively simple isotropic modeling approaches for electrokinetic phenomena, and provide important insights into structure-function relationships in cartilage matrix.

Several observations consistently supported the accuracy of our methods, and the conclusion that $\mathbf{k}_e$ was isotropic. The electrokinetic coupling coefficients obtained in this study (Fig. 4) correspond well with previous measurements using different techniques and cartilage sources (5,20,36). No systematic deviation from linearity of Q versus I was evident (Fig. 3 *b*), indicating that neither ohmic heating (which might introduce current-dependent behavior) nor explant degradation (which might introduce time-dependence of measured properties) significantly affected results. The main technical problems encountered during apparatus development were associated with temperature fluctuations, but this seemed well controlled as indicated by negligible fluid flow at zero current (Fig. 3 *b*). When current was switched between axial and radial directions, fluid outflow also switched without detectable changes in magnitude, indicating that $\mathbf{k}_e$ was isotropic. Had $\mathbf{k}_e$ been significantly anisotropic, fluid pressure fields within explants would have changed when current was changed, as pressure-driven flows would have been required to compensate for differences between electroosmotic inflows and outflows. However, no evidence for this was observed. Fluid outflow was always restricted to the direction of current flow, which would not be expected for pressure-driven flows. Furthermore, since fluid flows associated with these changing currents were easily large enough to induce significant matrix deformations had they been pressure-driven (30), the absence of visible explant deformations provided further evidence that pressure gradients did not in fact arise, and that $\mathbf{k}_e$ was indeed isotropic.

Isotropy of $\mathbf{k}_e$ contrasts with anisotropy of hydraulic permeability in compressed cartilage (30), but has an intuitive basis when considered in light of molecular-scale physics. Modeling of cartilage matrix microstructural deformations indicates that effective pore sizes can become direction-dependent with compression (29), contributing to the emergence of anisotropic hydraulic permeability. In a 1-D description of electrokinetic transport through membranes containing perpendicular cylindrical pores of radius r at volume fraction α filled with saline of viscosity η, previous investigators have obtained analytical expressions for electrokinetic coupling matrices analogous to that of Eq. 1 (37). For the approximation of a "Helmholtz double layer" (arising from fixed surface charge density within pores) characterized by thickness $d \ll r$ and electrostatic potential ζ at the pore wall, these results may be written

$$\begin{bmatrix} \mathbf{U} \\ \mathbf{J} \end{bmatrix} = \alpha \begin{bmatrix} -\dfrac{r^2}{8\eta} & \dfrac{\varepsilon\zeta}{\eta} \\ \dfrac{\varepsilon\zeta}{\eta} & -\left(\sigma + \dfrac{2\varepsilon^2\zeta^2}{r\eta d}\right) \end{bmatrix} \cdot \begin{bmatrix} \nabla p \\ \nabla \phi \end{bmatrix}, \qquad (10)$$

where ε and σ represent dielectric permittivity and electric conductivity of saline. As indicated by its dependence upon r^2, the hydraulic permeability (term in Eq. 10 corresponding to $\mathbf{K}_{11}$ in Eq. 1) is sensitive to the pore geometry. In contrast, $\mathbf{K}_{12}$ and $\mathbf{K}_{21}$ exhibit no r-dependence whereas $\mathbf{K}_{22}$ has relatively weak r-dependence (Eq. 10), suggesting that these properties are less affected by changes in pore structure. Similar insights also emerge from more geometrically complex modeling of electrokinetic transport in cartilage, where fluid flow and electric current through the interstices of a random array of charged solid cylinders (representing gylcosaminoglycans) was considered (31,38). This work indicates that changing matrix density will have relatively greater effects on hydraulic permeability than on electrokinetic transport coefficients (31,38). It is therefore reasonable that direction-dependent changes in matrix structure that underlie the emergence of anisotropic hydraulic permeability ($\mathbf{K}_{11}$) in compressed cartilage may not measurably affect the isotropy of $\mathbf{K}_{12}$, $\mathbf{K}_{21}$, or $\mathbf{K}_{22}$. Similarly, tissues bearing significant structural anisotropy even when undeformed, such as the cartilage superficial zone, might reasonably be expected to exhibit anisotropic $\mathbf{K}_{11}$, but isotropic $\mathbf{K}_{12}$, $\mathbf{K}_{21}$, and $\mathbf{K}_{22}$.

Results for the relatively weak dependence of $\mathbf{k}_e$ on compression (Fig. 4) also followed predictions of microstructure-based models. Increased matrix density due to cartilage compression is expected to induce modest decreases in the magnitude of K_{12}^x and increases in K_{22}^x (31,38). Consistent with these predictions, the magnitudes of k_e^z and k_e^r (Eq. 3) were found to decrease somewhat with increasing compression (Fig. 4).

Findings of isotropic $\mathbf{k}_e$ may provide insights into mediators of chondrocyte biological responses to cartilage compression, and help refine application of electrically based assessment of cartilage integrity. The extracellular matrix of articular cartilage may be expected to acquire anisotropic transport properties during tissue compression, due to

direction-dependent changes in molecular architecture (29). This emergent anisotropy (30) may mediate direction-dependent pericellular matrix deposition in compressed cartilage (28). The isotropy exhibited by $\mathbf{k}_e$ in compressed cartilage would therefore argue against contributions from matrix electrokinetic properties as microphysical mediators of direction-dependent chondrocyte behavior (28). Immobilized glycosaminoglycans provide most of the fixed charge density, which gives rise to electrokinetic phenomena in cartilage. Since $\mathbf{k}_e$ is isotropic and relatively insensitive to matrix deformations, it may provide an indicator of immobolized glycosaminoglycan content that is more robust to different tissue loading conditions and measurement configurations than other cartilage material properties such as hydraulic permeability (30). These findings of directional invariance of $\mathbf{k}_e$ also justify relatively simple isotropic modeling of cartilage electrokinetic behavior (20–22), which may help improve clinical diagnosis of cartilage disease (15–19).

This work was supported by a grant from the Swiss National Science Foundation. We also thank Mr. Paulo Germano for help with electronic design.

REFERENCES

1. Maroudas, A. 1975. Biophysical chemistry of cartilaginous tissues with special reference to solute and fluid transport. *Biorheology.* 12:233–248.
2. Grodzinsky, A. J. 1983. Electromechanical and physicochemical properties of connective tissues. *Crit. Rev. Biomed. Eng.* 9:133–199.
3. Frank, E. H., and A. J. Grodzinsky. 1987. Cartilage electromechanics. I. Electrokinetic transduction and the effects of electrolyte pH and ionic strength. *J. Biomech.* 20:615–627.
4. Chen, A. C., W. C. Bae, R. M. Schinagl, and R. L. Sah. 2001. Depth- and strain-dependent mechanical and electromechanical properties of full-thickness bovine articular cartilage in confined compression. *J. Biomech.* 34:1–12.
5. Garcia, A. M., E. H. Frank, P. E. Grimshaw, and A. J. Grodzinsky. 1996. Contributions of fluid convection and electrical migration to transport in cartilage: relevance to loading. *Arch. Biochem. Biophys.* 333:317–325.
6. Levich, V. G. 1962. Physicochemical Hydrodynamics. Prentice-Hall, Englewood Cliffs, NJ.
7. Melcher, J. R. 1981. Continuum Electromechanics. The MIT Press, Cambridge, MA.
8. Beebe, D. J., G. A. Mensing, and G. M. Walker. 2002. Physics and applications of microfluidics in biology. *Annu. Rev. Biomed. Eng.* 4:261–286.
9. Grimshaw, P. E., A. J. Grodzinsky, M. L. Yarmush, and D. M. Yarmush. 1990. Selective augmentation of macromolecular transport in gels by electrodiffusion and electrokinetics. *Chem. Eng. Sci.* 45:2917–2929.
10. Probstein, R. F., and R. E. Hicks. 1993. Removal of contaminants from soils by electric fields. *Science.* 260:498–503.
11. Dhopeshwarkar, R., L. Sun, and R. M. Crooks. 2005. Electrokinetic concentration enrichment within a microfluidic device using a hydrogel microplug. *Lab Chip.* 5:1148–1154.
12. Frank, E. H., A. J. Grodzinsky, T. J. Koob, and D. R. Eyre. 1987. Streaming potentials: a sensitive index of enzymatic degradation in cartilage. *J. Orthop. Res.* 5:497–508.
13. Bonassar, L. J., J. D. Sandy, M. W. Lark, A. H. Plaas, E. H. Frank, and A. J. Grodzinsky. 1997. Inhibition of cartilage degradation and changes in physical properties induced by IL-1beta and retinoic acid using matrix metalloproteinase inhibitors. *Arch. Biochem. Biophys.* 344:404–412.
14. Mankin, H. J., and K. D. Brandt. 1984. Biochemistry and metabolism of cartilage in osteoarthritis. *In* Osteoarthritis. R. W. Moskowitz, D. S. Howell, V. M. Goldberg, and H. J. Mankin, editors. WB Saunders, Philadelphia, PA. 43–79.
15. Berkenblit, S. I., E. H. Frank, E. P. Salant, and A. J. Grodzinsky. 1994. Nondestructive detection of cartilage degeneration using electromechanical surface spectroscopy. *J. Biomech. Eng.* 116:384–392.
16. Minassian, A., D. O'Hare, K. H. Parker, J. P. Urban, K. Warensjo, and C. P. Winlove. 1998. Measurement of the charge properties of articular cartilage by an electrokinetic method. *J. Orthop. Res.* 16:720–725.
17. Legare, A., M. Garon, R. Guardo, P. Savard, A. R. Poole, and M. D. Buschmann. 2002. Detection and analysis of cartilage degeneration by spatially resolved streaming potentials. *J. Orthop. Res.* 20: 819–826.
18. Frank, E., R. Evans, C. Lee, S. Treppo, M. Spector, and A. Grodzinsky. 2004. Quantitative electrical impedance analysis of cartilage degradation. *Biorheology.* 41:195–202.
19. Binette, J. S., M. Garon, P. Savard, M. D. McKee, and M. D. Buschmann. 2004. Tetrapolar measurement of electrical conductivity and thickness of articular cartilage. *J. Biomech. Eng.* 126:475–484.
20. Frank, E. H., and A. J. Grodzinsky. 1987. Cartilage electromechanics. II. A continuum model of cartilage electrokinetics and correlation with experiments. *J. Biomech.* 20:629–639.
21. Sachs, J. R., and A. J. Grodzinsky. 1989. An electromechanically coupled poroelastic medium driven by an applied electric current: surface detection of bulk material properties. *Physicochemical Hydrodynamics.* 11:585–614.
22. Kojic, M., N. Filipovic, and S. Mijailovic. 2001. A large strain finite element analysis of cartilage deformation with electrokinetic coupling. *Comput. Methods Appl. Mech. Eng.* 190:2447–2464.
23. Kim, Y. J., L. J. Bonassar, and A. J. Grodzinsky. 1995. The role of cartilage streaming potential, fluid flow, and pressure in the stimulation of chondrocyte biosynthesis during dynamic compression. *J. Biomech.* 28:1055–1066.
24. Torzilli, P. A., J. M. Arduino, J. D. Gregory, and M. Bansal. 1997. Effect of proteoglycan removal on solute mobility in articular cartilage. *J. Biomech.* 30:895–902.
25. Leddy, H. A., and F. Guilak. 2003. Site-specific molecular diffusion in articular cartilage measured using fluorescence recovery after photobleaching. *Ann. Biomed. Eng.* 31:753–760.
26. Sniekers, Y. H., and C. C. van Donkelaar. 2005. Determining diffusion coefficients in inhomogeneous tissues using fluorescence recovery after photobleaching. *Biophys. J.* 89:1302–1307.
27. Evans, R. C., and T. M. Quinn. 2006. Solute convection in dynamically compressed cartilage. *J. Biomech.* 39:1048–1055.
28. Quinn, T. M., A. J. Grodzinsky, M. D. Buschmann, Y. J. Kim, and E. B. Hunziker. 1998. Mechanical compression alters proteoglycan deposition and matrix deformation around individual cells in cartilage explants. *J. Cell Sci.* 111:573–583.
29. Quinn, T. M., P. Dierickx, and A. J. Grodzinsky. 2001. Glycosaminoglycan network geometry may contribute to anisotropic hydraulic permeability in cartilage under compression. *J. Biomech.* 34:1483–1490.
30. Reynaud, B., and T. M. Quinn. 2006. Anisotropic hydraulic permeability in compressed articular cartilage. *J. Biomech.* 39:131–137.
31. Eisenberg, S. R., and A. J. Grodzinsky. 1988. Electrokinetic micromodel of extracellular matrix and other polyelectrolyte networks. *Physicochemical Hydrodynamics.* 10:517–539.
32. Mow, V. C., and X. E. Guo. 2002. Mechano-electrochemical properties of articular cartilage: their inhomogeneities and anisotropies. *Annu. Rev. Biomed. Eng.* 4:175–209.

33. Press, W. H., B. P. Flannery, S. A. Teukolsky, and W. T. Vetterling. 1988. Numerical Recipes in C. Cambridge University Press, New York.

34. de Groot, S., and P. Mazur. 1962. Non-equilibrium thermodynamics. North-Holland Publishers, Amsterdam, The Netherlands.

35. Katchalsky, A., and P. F. Curran. 1981. Nonequilibrium thermodynamics in biophysics. Harvard University Press, Cambridge, MA.

36. Treppo, S., H. Koepp, E. C. Quan, A. A. Cole, K. E. Kuettner, and A. J. Grodzinsky. 2000. Comparison of biomechanical and biochemical properties of cartilage from human knee and ankle pairs. *J. Orthop. Res.* 18:739–748.

37. Grodzinsky, A. J., and J. R. Melcher. 1976. Electromechanical transduction with charged polyelectrolyte membranes. *IEEE Trans. Biomed. Eng.* 23:421–433.

38. Chammas, P., W. J. Federspiel, and S. R. Eisenberg. 1994. A microcontinuum model of electrokinetic coupling in the extracellular matrix: perturbation formulation and solution. *J. Colloid Interface Sci.* 168: 526–538.